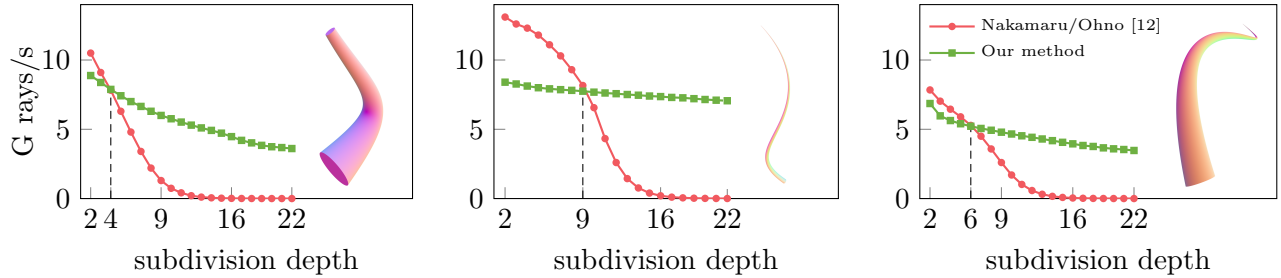


# Fast, High Precision Ray/Fiber Intersection using Tight, Disjoint Bounding Volumes

Nikolaus Binder, Alexander Keller

NVIDIA



**Figure 1:** The performance of methods pruning with (overlapping) AABBs drops dramatically with increasing subdivision depth, whereas our tight, disjoint bounding volumes always allow for efficient pruning and instant termination.

## Abstract

Analyzing and identifying the shortcomings of current subdivision methods for finding intersections of rays with fibers defined by the surface of a circular contour swept along a Bézier curve, we present a new algorithm that improves precision and performance. Instead of the inefficient pruning using overlapping axis aligned bounding boxes and determining the closest point of approach of the ray and the curve, we prune using disjoint bounding volumes defined by cylinders and calculate the intersections on the limit surface. This in turn allows for computing accurate parametric position and normal in the point of intersection. The iteration requires only one bit per subdivision to avoid costly stack memory operations. At a low number of subdivisions, the performance of the high precision algorithm is competitive, while for a high number of subdivisions it dramatically outperforms the state-of-the-art. Besides an extensive mathematical analysis, source code is provided.

## 1 Introduction

State-of-the-art photo realistic image synthesis is based on (quasi-) Monte Carlo simulation of light propagation: Rays are traced to connect the camera with the light sources. Then, the contribution of all these light paths is summed up.

Often, fibers for hair and fur are part of the scenery. These fibers are usually modeled as sweep surfaces along Bézier curves with a circular cross section and a parametric radius, which may vary along the curve. While triangles are a very common representation for most other parts of the scene geometry, they often are a very unsuitable approximation for fibers. Reasons for this exception include memory restrictions, numerical issues, and efficiency considerations. Therefore, especially in high quality rendering, custom primitives are used for fibers, and intersections of rays with these primitives must be found.

## 2 Previous Work

Most popular approaches are based on recursive subdivision of the curve [Cat74], after which either the segment of the curve can be approximated by a simple primitive or an iterative solver refines the solution. The number of subdivisions required for a certain reduction of curvature can be reduced by a more thorough analysis, however at the price of a significantly increased effort [HARL05].

Generalized cylinders [BB82] are a common representation for hair fibers. They are defined by sweeping an arbitrary two-dimensional contour along a three-dimensional curve. Intersections of rays with these objects can be found without tessellation [BK85]: Each ray is projected into a parametric frame aligned to the trajectory of the curve, i.e. the contour is fixed. At the same time the trajectory of the ray becomes a two-dimensional curve. Then, the ray and the contour are subdivided simultaneously until the size of their bounding boxes fall below a threshold. During the process, combinations of the two intervals for which the bounding boxes do not overlap can be pruned. In a final step, the exact intersection points are calculated, which requires solving equations of higher polynomial degree.

The method can be simplified by either restricting the shape of the sweep curve [vW84] or the shape of the contour without subdividing the curve first [vW85]. However, finding roots of polynomials with a high degree is still required and remains numerically challenging.

Intersections of rays and sweep surfaces with a circular cross section can also be found by combining the equations of the trajectory of a ray and the parametric distance of a point to a parametric position on the curve [Lei95]. Again, roots of a polynomial with high degree must be found.

Approximating the intersection on the surface of the fiber with the closest point of approach of the ray and the curve lowers the polynomial degree. The closest point of approach of two lines can be determined very efficiently in ray-centric coordinate systems using an adaptive linearization method based on recursive subdivision [NO02]. If only primary visibility from a pin hole camera is of concern, it can be beneficial to compute line samples instead of point samples [BGA12]. In the same spirit, cone tracing can decrease the number of samples significantly [QCH<sup>+</sup>14]. The obtained coverage information, however, may not fit the architecture of a fully path traced simulation.

Improvements of a “top level” hierarchy referencing fibers and unrolling curve subdivision such that the number of segments matches the SIMD width may improve performance on certain architectures [WBW<sup>+</sup>14]. More recent iterative root finding methods can replace recursive subdivision to improve convergence speed and precision at the same time [Res17].

While these methods computing the closest point of approach deliver state-of-the-art performance for a certain level of detail, they all suffer from the underlying approximation, which prohibits the determination of the correct intersection on the surface of the fiber and the normal in the intersection. An example for this issue is shown in Figure 2. Furthermore, the inefficiency of the pruning tests of subdivision-based methods becomes prohibitive for a high number of subdivisions. Finally, recursive methods using a stack suffer from memory bandwidth limitations, especially on current GPUs.

Fast ray tracing is possible due to efficient data structures that identify all potential parts of the scene that may be intersected by a ray. The state-of-the-art for these acceleration data structures performs hierarchical partitioning of either space or the set of objects. Furthermore, there exist hybrid schemes that partition both the set of objects and space in order to improve performance [SFD09]. As the construction and traversal of such acceleration data structures is almost orthogonal to the actual ray/fiber intersection, we focus on improving the latter in this article.



**Figure 2:** Left: Methods based on the closest point of approach cannot determine the correct parametric position and normal. Right: Our method computes both with high precision.

### 3 Algorithm

Our algorithm is a member of the family of subdivision-based methods computing intersections of rays with fibers by recursively bisecting the curve and pruning regions that cannot be intersected by the ray [Cat74].

The first contribution is a stackless iterative variant that only keeps track of subdivision levels that require backtracking and re-computes all necessary data instead of employing a stack. Our second contribution is a fast pruning test with oriented cylinders that significantly improves the accuracy, especially for a high number of subdivisions. After a termination criterion is met, e.g. a fixed number of subdivisions, the final intersection with the linearized segment, represented by a cylinder with oriented end caps, is computed. As bounding cylinders of neighboring curve segments now are disjoint by construction and closer segments are always intersected first, our algorithm can immediately terminate after an intersection has been found (3rd contribution). Instead of approximating the actual intersection on the surface of the fiber with the closest point of approach, we reuse the intersection already determined for pruning (4rd contribution) and are able to compute an accurate normal (5th contribution).

#### 3.1 Numerically Robust Curve Representation

A naïve implementation for cubic Bézier curves using four control points  $(p_0, p_1, p_2, p_3)$  suffers from severe floating point precision issues in our algorithm due to cancellation in differences required to determine the cylinder axis  $(p_3 - p_0)$  and the tangent in the split point.

Therefore, we use a representation tailored to our pruning test as illustrated in Figure 3: We maintain the first control point  $p := p_0$ , the tangents in the start and end points  $t_0 := p_1 - p_0, t_1 := p_3 - p_2$ , and the direction  $d := p_3 - p_0$ . This representation requires different rules for the subdivision of  $(p, d, t_0, t_1)$  into  $(p^L, d^L, t_0^L, t_1^L)$  and  $(p^R, d^R, t_0^R, t_1^R)$ , where

$$\begin{aligned}\Delta p &= \frac{3}{8}t_0 + \frac{1}{2}d - \frac{3}{8}t_1, \\ t_c &= -\frac{1}{8}t_0 + \frac{1}{4}d - \frac{1}{8}t_1,\end{aligned}$$

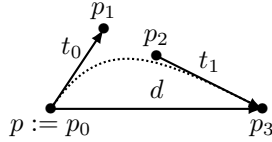


**Figure 3:** Representing the curve with the tuple  $\{\mathbf{p}, \mathbf{d}, \mathbf{t}_0, \mathbf{t}_1\}$  improves the numerical robustness of the method significantly.

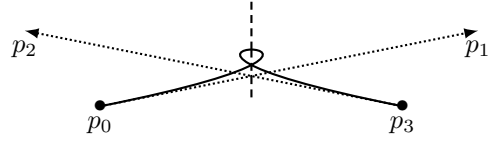


**Figure 4:** A loop violating the constraints required to construct disjoint bounding volumes must be split beforehand.

and

$$\begin{aligned}
 p^L &= p, & p^R &= p + \Delta p, \\
 d^L &= \Delta p, & d^R &= d - \Delta p, \\
 t_0^L &= \frac{1}{2}t_0, & t_0^R &= t_c, \\
 t_1^L &= t_c, & t_1^R &= \frac{1}{2}t_1.
 \end{aligned}$$

As we will use disjoint bounding volumes, only one of the two sets needs to be calculated as determined by the pruning test. In fact this subdivision can be computed even slightly more efficiently than the subdivision of  $(p_0, p_1, p_2, p_3)$  and only exposes a minimal amount of instruction divergence due to branching.

### 3.2 Efficient Hierarchical Pruning

Each region of the subdivision is conservatively bounded by an oriented cylinder, which is partitioned by a plane located in the split point and perpendicular to the tangent in the split point of the curves. The limit surface of these cylinders guarantees that an intersection is always mapped to the closest point on the curve.

Only if the intersection of the ray with the plane is inside the cylinder, both sub-regions must be considered. Then, subdivision starts with the region whose bounding volume is intersected first along the ray. Figure 5 shows an example with four possible cases. Note that the test for inclusion only requires comparing the distances of the two ray/cylinder intersections with the distance of the intersection with the plane.

As these pruning tests are performed with disjoint bounding volumes and refinement always continues with the closest sub-region, subdivision can immediately terminate after an intersection has been found. Instant termination is essential for a high number of subdivisions because otherwise the number of unpruned regions may grow exponentially with subdivision depth.

While bounding both subcurves in individual cylinders instead of using one partitioned cylinder improves the culling accuracy, the overhead of computing and intersecting two bounding volumes outweighs the theoretical benefit in practice, especially since the benefit quickly decreases with subdivision.

### 3.3 Implementation

Pruning is performed in a ray centric coordinate system, in which the ray starts in the origin and goes along the positive  $z$  axis (“unit ray”). A reliable orthonormal basis can be efficiently constructed using Duff et al.’s recent improvement of Frisvad’s method [Fri12, DBC<sup>+</sup>17]. The transformation into the local frame only needs to be performed once at the beginning by calculating a local set of

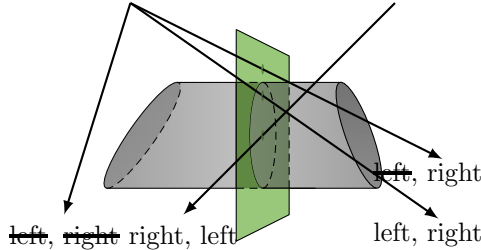


**Figure 5:** Bounding cylinders with partitioning planes improve the efficiency of pruning tests and allow for instant termination after an intersection has been found.

control points. In this coordinate system, we can simplify ray/plane intersection and the infinite cylinder intersection described by Cychosz et al. [CW94] significantly since  $\forall v \in \mathbb{R}^3: \langle v, d \rangle = v_z$  and  $v - o = v$  for a unit ray defined by its origin and direction  $(o, d)$ . Listings 1 and 2 present the resulting optimized intersection functions; the simplified ray/cylinder intersection is derived in Appendix A.

We use four-dimensional control points, where the first three components are the position, and the last one defines the radius. This consistent representation allows for cubic interpolation of the radius.

Bounding cylinders are oriented along the vector connecting the first and last control point and have a conservative radius defined by the sum of the maximum radius in the region and the maximum distance of the inner control points to the cylinder axis. We also use Bézier curves for radius interpolation, and bound the parametric radius using the convex hull property.

An example implementation for the computation of a conservative radius for the bounding cylinders and cubic Bézier curves is given in Listing 8, using the distance of the two inner control points to the axis determined by the method shown in Listing 3.

The infinite cylinders are cropped by restricting the  $t$ -parameter interval of the ray. After determining initial bounds of the  $t$  parameter interval, in each subdivision step one of the interval bounds is updated; both are recalculated after backtracking. A simple implementation for cubic Bézier curves is shown in Listing 6.

Recursive subdivision is performed by an iterative process by maintaining a bit string in which each subdivision level is represented by one bit and the current size of the parametric domain. After the pruning test, the corresponding bit in the bit string is set to one if and only if both subregions must be considered, and only in this case backtracking is required. Then, the control points and the  $t$  interval are recalculated to avoid maintaining a stack of control points. The current parametric interval of the curve can directly be derived from the bit stack. It is always maintained in two integer variables for start and size of the interval, which must be converted to floating point values in the unit interval before calculating new control points. This conversion is shown in Listing 4.

Upon termination, the intersection of the ray with the bounding cylinder used for pruning already determines the intersection with the linearized segment. Only very little effort is required to compute the normal and the parametric value in the intersection, and this calculation is performed by all threads of a warp simultaneously in the very end. Listing 13 shows a possible implementation.

### 3.4 Constraints and Limitations

A bisection into subregions that can be bounded by disjoint bounding volumes poses well-defined restrictions on the allowed sets of control points. At the same time, the constraints also ensure that curves with valid configurations cannot be split into invalid ones. For cubic Bézier curves the

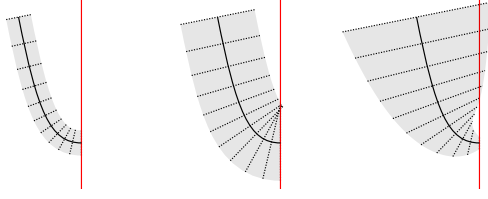


**Figure 6:** While curves may be split disjointly in cusps, thicker fibers can still overlap splitting planes, causing visible defects. While the left fiber does not suffer from this issue, the fiber in the middle, which goes along the same curve but has a larger radius does. Of course, fibers with parametric radius (right) can also overlap partitioning planes.

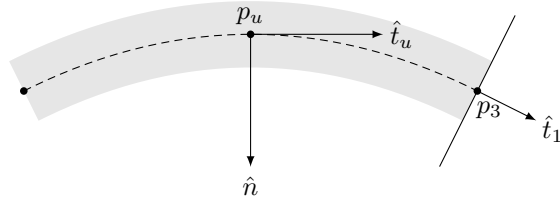


**Figure 7:** Illustration of finding the closest point on the normal plane in a point on the curve to a partitioning plane.

constraints

$$\begin{aligned}
 \langle p_2 - p_0, p_1 - p_0 \rangle &\geq 0, \\
 \langle p_3 - p_1, p_1 - p_0 \rangle &\geq 0, \\
 \langle p_3 - p_1, p_3 - p_2 \rangle &\geq 0, \\
 \langle p_2 - p_0, p_3 - p_2 \rangle &\geq 0, \\
 \langle p_2 - p_0, p_3 - p_1 \rangle &\geq 0
 \end{aligned}$$

guarantee that the curve can be recursively split into subcurves with disjoint bounding volumes. Appendix B provides the constraints required for quadratic Bézier curves and all necessary proofs for both quadratic and cubic Bézier curves. Curves that do not fulfill these constraints must be subdivided beforehand. An example for such a configuration is shown in Figure 4.

While these constraints are necessary, they are not sufficient to guarantee disjoint bounding volumes of fibers: If a point on the surface (perpendicular to the tangent  $t_u$  of the point on the curve  $p_u$ , at a distance defined by the radius in that point  $r_u$ ) intersects the partitioning plane in the split point, a valid part of the surface of the fiber will be cropped.

Figure 6 shows three examples: The leftmost fiber with a small, constant radius does not suffer from this issue, while the surface of the other ones intersects the split plane as their radius is too large, and thus errors may be introduced. Besides thick fibers, high curvatures (e.g. in cusps) can cause similar issues. Regions with such a behavior must be isolated and require subdivision beforehand, too. Note that a similar issue affects methods based on the closest point of approach.

Such configurations can be identified as shown in Figure 7: The surface point closest to the plane in the split point perpendicular to the split tangent  $t_1$  is on the plane perpendicular to the tangent  $t$  at the parametric position. Gram-Schmidt orthogonalization yields the displacement from the

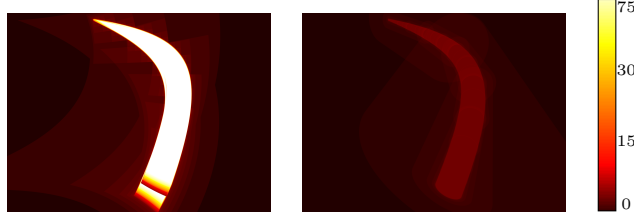


**Figure 8:** Pruning with oriented cylinders (right) dramatically lowers the total number of regions of interest by reducing the number false positives compared to pruning with axis aligned bounding boxes (left), especially for a high number of subdivisions.

curve closest to the split plane

$$\begin{aligned}
 n_u &= t_1 - \langle t_1, \hat{t}_u \rangle \cdot \hat{t}_u \\
 &= t_1 - \frac{\langle t_1, t_u \rangle t_u}{\langle t_u, t_u \rangle} \\
 &\propto \langle t_u, t_u \rangle t_1 - \langle t_1, t_u \rangle t_u,
 \end{aligned}$$

where  $t_u = (1 - u)^2(p_1 - p_0) + 2(1 - u)u(p_2 - p_1) + u^2(p_3 - p_2)$  and  $t_1 = p_3 - p_2$  for a cubic Bézier curve. As  $n_u$  has a maximum degree of 4, checking all solutions  $u_i \in [0, 1]$  of

$$\begin{aligned}
 \langle p_3 - p_u + r_u \cdot \hat{n}_u, \hat{t}_1 \rangle &= 0 && \text{or just} \\
 \langle p_3 - p_u + \bar{r} \cdot \hat{n}_u, \hat{t}_1 \rangle &= 0, && r_u \leq \bar{r}
 \end{aligned}$$

requires solving a quartic equation, e.g. using Ferrari’s method [Smi29], eliminating the cubic term using the Tschirnhaus transformation [Boy68].

As the curvature decreases with subdivision (see subdivision rules in Section 3.1) and the maximum radius  $\bar{r}$  is a constant, it is sufficient to check each fiber only initially in its two end points with corresponding tangents.

While it would be trivially possible to support all possible curve configurations and overcome the issues in cusps and with very thick fibers by optionally allowing overlapping bounding volumes in certain subdivisions, the overhead of checking the criteria in every subdivision step and recording the ones that overlap will most likely not pay off in practice since the number of such configurations is usually small. As furthermore the cost of splitting beforehand is rather moderate, the overall penalty tends to be negligible.

## 4 Results and Discussion

We evaluated the performance and precision of the presented algorithm using single fibers along quadratic and cubic Bézier curves.

Figure 8 compares the number of pruning tests required for our method to pruning with axis aligned bounding boxes for a high number of subdivisions. As expected the overlapping axis aligned bounding boxes result in an exponential growth of regions that cannot be pruned. Note that the bounding boxes are aligned to the main axis of the coordinate system of each ray, hence they appear to be warped.

Figure 1 shows the performance for intersecting  $\sim 1$  million rays with a single fiber on an NVIDIA Titan V. While the relative performance does depend on the orientation and curvature of the fiber, as pruning with axis aligned bounding boxes benefits from straight, aligned fibers, the main issue for the dramatic slowdown of the state-of-the art remains: After a certain number of subdivisions,

the bounding boxes of two curves resulting from the subdivision of a region overlap almost entirely. Then, none of them can be pruned and a significant amount of additional backtracking is required.

Nakamaru’s method [NO02] does not take into account the ray direction for deciding which subcurve is checked first, therefore causing exponential growth of valid regions in the worst case. Hybrids between the two methods, i.e. pruning with axis aligned bounding boxes, taking ray direction into account, and calculating the final intersection with cylinders not only suffer from divergence caused by the additional test, but are mostly limited by the pruning inefficiency, and therefore may be only valuable in rare cases.

Combining the fiber intersection with a top level hierarchy referencing fibers, or regions on fibers if the fiber must be split beforehand, is straightforward. The top level hierarchy is primarily orthogonal to fiber intersection unless fibers are partitioned into very small regions. Then, the increased efficiency of the pruning tests of the presented method becomes even more important.

Note that in practice, intersection cost is almost always dominated by the performance of traversing the hierarchy referencing the fibers and other geometry in the scene. Nevertheless, we calculate accurate intersections and normals on the surface in a reliable way and do so either with a small overhead or – if high precision is of concern – dramatically faster.

## 5 Conclusion

We have presented an algorithm that outperforms the state-of-the-art subdivision-based ray/fiber intersection method significantly for a high number of subdivisions, and computes accurate intersections on the surface of the fiber with an accurate normal. In addition, we also determine a precise parametric position. Even for small numbers of subdivisions, which quite often lead to visible artifacts in Nakamaru’s method [NO02], the approximation error of our algorithm is well understood and the overhead of pruning with oriented cylinders instead of axis aligned bounding boxes remains reasonable. While the algorithm cannot handle arbitrary fibers, configurations that cannot be supported can be identified in advance. Subdividing such fibers resolves the issues.

Future opportunities include displacements and arbitrary contours, both only requiring an additional intersection test after pruning with conservative bounding cylinders.

## References

- [BB82] D. Ballard and C. Brown. *Computer Vision*. Prentice Hall Professional Technical Reference, 1st edition, 1982.
- [BGA12] R. Barringer, C. Gribel, and T. Akenine-Möller. High-quality curve rendering using line sampled visibility. *ACM Trans. Graph.*, 31(6):162:1–162:10, 2012.
- [BK85] W. Bronsvoort and F. Klok. Ray tracing generalized cylinders. *ACM Trans. Graph.*, 4(4):291–303, October 1985.
- [Boy68] C. Boyer. *A History of Mathematics*. Wiley, New York, 1968.
- [Cat74] E. Catmull. *A Subdivision Algorithm for Computer Display of Curved Surfaces*. PhD thesis, The University of Utah, 1974. AAI7504786.
- [CW94] J. Cychosz and W. Waggenspack, Jr. Intersecting a ray with a cylinder. In Paul S. Heckbert, editor, *Graphics Gems IV*, pages 356–365. Academic Press Professional, Inc., San Diego, CA, USA, 1994.

- [DBC<sup>+</sup>17] T. Duff, J. Burgess, P. Christensen, C. Hery, A. Kensler, M. Liani, and R. Villemin. Building an orthonormal basis, revisited. *Journal of Computer Graphics Techniques (JCGT)*, 6(1):1–8, 2017.
- [dC59] P. de Casteljaou. Outillages methodes calcul. Technical report, Citroën France, 1959.
- [Fri12] J. Frisvad. Building an orthonormal basis from a 3d unit vector without normalization. *Journal of Graphics Tools*, 16(3):151–159, 2012.
- [HARL05] T. Hain, A. Ahmad, S. Racherla, and D. Langan. Fast, precise flattening of cubic bézier path and offset curves. *Comput. Graph.*, 29(5):656–666, October 2005.
- [Lei95] A. Leipelt. Ray tracing a swept sphere. In Alan W. Paeth, editor, *Graphics Gems V*, pages 258–267. Academic Press, 1995.
- [NO02] K. Nakamaru and Y. Ohno. Ray tracing for curves primitive. In *WSCG*, pages 311–316, 2002.
- [QCH<sup>+</sup>14] H. Qin, M. Chai, Q. Hou, Z. Ren, and K. Zhou. Cone tracing for furry object rendering. *IEEE Transactions on Visualization and Computer Graphics*, 20(8):1178–1188, August 2014.
- [Res17] A. Reshetov. Exploiting budan-fourier and vincent’s theorems for ray tracing 3d bézier curves. In *Proceedings of High Performance Graphics, HPG ’17*, pages 5:1–5:11, New York, NY, USA, 2017. ACM.
- [SFD09] M. Stich, H. Friedrich, and A. Dietrich. Spatial splits in bounding volume hierarchies. In *Proceedings of the Conference on High Performance Graphics 2009, HPG ’09*, pages 7–13, New York, NY, USA, 2009. ACM.
- [Smi29] D. Smith. *A Source Book in Mathematics*. McGraw-Hill Book Company, Inc., London, 1929.
- [vW84] J. van Wijk. Ray tracing objects defined by sweeping planar cubic splines. *ACM Trans. Graph.*, 3(3):223–237, July 1984.
- [vW85] J. van Wijk. Ray tracing objects defined by sweeping a sphere. *Computers & Graphics*, 9(3):283–290, 1985.
- [WBW<sup>+</sup>14] S. Woop, C. Benthin, I. Wald, G. Johnson, and E. Tabellion. Exploiting local orientation similarity for efficient ray traversal of hair and fur. In *Proceedings of High Performance Graphics, HPG ’14*, pages 41–49, Aire-la-Ville, Switzerland, Switzerland, 2014. Eurographics Association.

## Appendix A: Intersection of a unit ray with an infinite cylinder

The ray/cylinder intersection described by Cychosz et al [CW94] can be simplified for unit rays, because a normalization of the cylinder axis is not required:

The smallest distance between the ray and an infinite line through the points  $p$  and  $q$ , i.e. with axis  $A := q - p$ , normalized to  $\hat{A} := \frac{A}{|A|}$  is

$$d = |p \cdot D|, \text{ where}$$

$$D = \frac{\hat{R} \times \hat{A}}{|\hat{R} \times \hat{A}|}.$$

For  $\bar{l}_A := \frac{1}{|A|}$ ,

$$\hat{R} \times \hat{A} = \hat{R} \times (A \cdot \bar{l}_A) = (\hat{R} \times A) \cdot \bar{l}_A = (-a_y, a_x, 0)^T \cdot \bar{l}_A.$$

Furthermore,

$$|\hat{R} \times \hat{A}| = \sqrt{\bar{l}_A^2 (a_y^2 + a_x^2)} = \bar{l}_A \sqrt{a_x^2 + a_y^2}.$$

Therefore,

$$D = \frac{\hat{R} \times \hat{A}}{|\hat{R} \times \hat{A}|} = \frac{(-a_y, a_x, 0)^T \cdot \bar{l}_A}{\sqrt{a_x^2 + a_y^2} \cdot \bar{l}_A} = \frac{(-a_y, a_x, 0)^T}{\sqrt{a_x^2 + a_y^2}},$$

and the **squared** minimum distance between the ray and the line is

$$d^2 = \frac{(a_x p_y - a_y p_x)^2}{a_x^2 + a_y^2}. \quad (1)$$

The ray hits the infinite cylinder through  $p$  and  $q$  with the radius  $r$  if and only if

$$d^2 \leq r^2.$$

For the special cases of a line along the  $z$  axis, in which the denominator of (1) would be zero, the squared distance between the ray and the line is the two-dimensional distance of  $p$  to the origin, i.e.  $d^2 = p_x^2 + p_y^2$ .

Setting  $g := a_x^2 + a_y^2$ , the distance of the closest point of approach (cpa) of the ray and the cylinder

from the ray origin is

$$\begin{aligned}
t_{cpa} &= \frac{(p \times \hat{A}) \cdot D}{|\hat{R} \times \hat{A}|} \\
&= \frac{\bar{l}_A(p \times A) \cdot \frac{(-a_y, a_x, 0)^T}{\sqrt{g}}}{\bar{l}_A \sqrt{g}} \\
&= \frac{(p \times A) \cdot (-a_y, a_x, 0)^T}{g} \\
&= \frac{(p_y a_z - p_z a_y, p_z a_x - p_x a_z, p_x a_y - p_y a_x)^T \cdot (-a_y, a_x, 0)^T}{g} \\
&= \frac{-p_y a_y a_z + p_z a_y^2 + p_z a_x^2 - p_x a_z a_x}{g} \\
&= \frac{p_z g - a_z(p_y a_y + p_x a_x)}{g} \\
&= p_z - \frac{a_z(p_y a_y + p_x a_x)}{g}.
\end{aligned}$$

The intersections of the ray and the cylinder are located at  $(0, 0, t \pm s)$ , where

$$\begin{aligned}
s &= \left| \frac{\sqrt{r^2 - d^2}}{\hat{R} \cdot \hat{O}} \right| \quad \text{and} \\
\hat{O} &= \frac{D \times \hat{A}}{|D \times \hat{A}|}.
\end{aligned}$$

Again, a normalization of  $A$  is not required, as its inverse length  $\bar{l}_A$  cancels out:

$$\begin{aligned}
D \times \hat{A} &= \frac{(-a_y, a_x, 0)^T}{\sqrt{g}} \times (A \cdot \bar{l}_A) = ((-a_y, a_x, 0)^T \times A) \cdot \frac{\bar{l}_A}{\sqrt{g}} \\
&= (a_x a_z, a_y a_z, -g)^T \cdot \frac{\bar{l}_A}{\sqrt{g}},
\end{aligned}$$

Hence,

$$\begin{aligned}
|D \times \hat{A}| &= \sqrt{\frac{\bar{l}_A^2}{g^2} (a_x^2 a_z^2 + a_y^2 a_z^2 + g^2)} = \frac{\bar{l}_A}{\sqrt{g}} \sqrt{a_z^2 (a_x^2 + a_y^2) + g^2} \\
&= \frac{\bar{l}_A}{\sqrt{g}} \sqrt{a_z^2 g + g^2}, \\
\hat{O} &= \frac{(a_x a_z, a_y a_z, -g)^T}{\sqrt{a_z^2 g + g^2}} = \frac{(a_x a_z, a_y a_z, -g)^T}{\sqrt{g(a_z^2 + g)}}.
\end{aligned}$$

For a unit ray with  $\hat{R} = (0, 0, 1)^T$ , we only need to consider

$$O_z = -\frac{g}{\sqrt{g(a_z^2 + g)}} = -\sqrt{\frac{g}{a_z^2 + g}},$$

since all terms are positive. Finally,

$$s = \frac{\sqrt{r^2 - d^2}}{\sqrt{\frac{g}{a_z^2 + g}}} = \sqrt{\frac{r^2 - d^2}{\frac{g}{a_z^2 + g}}} = \sqrt{\frac{(r^2 - d^2)(a_z^2 + g)}{g}},$$

and the distance to the closest visible surface boundary is

$$t = \begin{cases} t_{cpa} - s & t_{cpa} \geq s \\ t_{cpa} + s & \text{otherwise.} \end{cases}$$

If  $t < 0$ , the cylinder is behind the ray origin.

## Appendix B: Curve Constraints

### B.1 Quadratic Bézier Curves

**Lemma 1.** The two subcurves defined by their control points  $(p_0^L, p_1^L, p_2^L)$  and  $(p_0^R, p_1^R, p_2^R)$  resulting from de Casteljau subdivision [dC59] in the domain center of the quadratic Bézier curve defined by the control points  $(p_0, p_1, p_2)$  can be enclosed by disjoint bounding volumes partitioned by a plane located in the split point  $s := \frac{p_0 + 2p_1 + p_2}{4}$  orthogonal to the tangent in the split point  $t := p_2 - p_0$  if and only if

$$\langle p_1 - p_0, p_1 - p_2 \rangle \leq 0. \quad (2)$$

**Proof.** As Bézier curves are defined as a convex combination of the control points, the bounding volumes of the two sub curves are disjointedly can be split by the plane located in  $s$  and orthogonal to  $t$  if

$$\langle p_i^L - s, t \rangle \leq 0 \quad \text{and} \quad (3)$$

$$\langle p_i^R - s, t \rangle \geq 0 \quad \forall i \in \{0, 1, 2\}. \quad (4)$$

De Casteljau subdivision in the domain center creates the control points

$$(p_0^L, p_1^L, p_2^L) := \left( p_0, \frac{p_0 + p_1}{2}, \frac{p_0 + 2p_1 + p_2}{4} \right) \quad \text{and}$$

$$(p_0^R, p_1^R, p_2^R) := \left( \frac{p_0 + 2p_1 + p_2}{4}, \frac{p_1 + p_2}{2}, p_2 \right)$$

of the two subcurves.

$p_2^L = p_0^R = s$  obviously fulfill the conditions by construction.

For  $p_0^L := p_0$

$$\begin{aligned} & \left\langle p_0 - \frac{p_0 + 2p_1 + p_2}{4}, p_2 - p_0 \right\rangle \leq 0 \\ \Leftrightarrow & \langle 3p_0 - 2p_1 - p_2, p_2 - p_0 \rangle \leq 0 \\ \Leftrightarrow & \underbrace{\langle p_0 - p_2, p_2 - p_0 \rangle}_{\leq 0} + \langle 2p_0 - 2p_1, p_2 - p_0 \rangle \leq 0 \\ \Leftrightarrow & \langle p_0 - p_1, p_2 - p_0 \rangle \leq 0. \end{aligned} \quad (5)$$

Analogously, checking  $p_2^R := p_2$  gives  $\langle p_1 - p_2, p_2 - p_0 \rangle \leq 0$ . The reversed conditions

$$\langle p_1 - p_0, p_2 - p_0 \rangle \geq 0 \quad \text{and} \quad (6)$$

$$\langle p_1 - p_2, p_0 - p_2 \rangle \geq 0 \quad (7)$$

can be combined to

$$\langle p_1 - p_0, p_1 - p_2 \rangle \leq 0, \quad (8)$$

as the projections of  $p_1 - p_0$  and  $p_1 - p_2$  onto  $p_2 - p_0$  must have different signs to satisfy both conditions (so that  $p_1$  is inside the hatched area in Figure 9).



**Figure 9:**  $p_1$  must be inside the hatched area if and only if (6) and (7) are satisfied. Only in that case (2) is also fulfilled.

Finally, for  $p_1^L := \frac{1}{2}p_0 + \frac{1}{2}p_1$  the conditions are always met, as

$$\begin{aligned}
& \langle p_1^L - s, t \rangle \leq 0 \\
\Leftrightarrow & \left\langle \frac{p_0 + p_1}{2} - \frac{p_0 + 2p_1 + p_2}{4}, p_2 - p_0 \right\rangle \leq 0 \\
\Leftrightarrow & \langle 2p_0 + 2p_1 - (p_0 + 2p_1 + p_2), p_2 - p_0 \rangle \leq 0 \\
\Leftrightarrow & \langle p_0 - p_2, p_2 - p_0 \rangle \leq 0. \tag{9}
\end{aligned}$$

The remaining proof for  $p_1^R$  is analogous. As all control points are now on one side of the splitting plane, their convex hull property ensures that all control points of further subcurves and the subcurve itself must also be on this side.  $\square$

**Lemma 2.** Splitting the quadratic Bézier curve fulfilling (2) in the domain center results in two subcurves that both also satisfy (2). Hence, all nested subcurves fulfill the condition.

**Proof.** For the left subcurve

$$\begin{aligned}
& \langle p_1^L - p_0^L, p_1^L - p_2^L \rangle \leq 0 \\
\Leftrightarrow & \left\langle \frac{p_0 + p_1}{2} - p_0, \frac{p_0 + p_1}{2} - \frac{p_0 + 2p_1 + p_2}{4} \right\rangle \leq 0 \\
\Leftrightarrow & \langle p_1 - p_0, 2p_0 + 2p_1 - p_0 - 2p_1 - p_2 \rangle \leq 0 \\
\Leftrightarrow & \underbrace{\langle p_1 - p_0, p_0 - p_2 \rangle}_{\geq 0 \text{ by Eq. (6)}} \leq 0,
\end{aligned}$$

and for the right subcurve

$$\begin{aligned}
& \langle p_1^R - p_0^R, p_1^R - p_2^R \rangle \leq 0 \\
\Leftrightarrow & \left\langle \frac{p_1 + p_2}{2} - \frac{p_0 + 2p_1 + p_2}{4}, \frac{p_1 + p_2}{2} - p_2 \right\rangle \leq 0 \\
\Leftrightarrow & \langle 2p_1 + 2p_2 - (p_0 + 2p_1 + p_2), p_1 + p_2 - 2p_2 \rangle \leq 0 \\
\Leftrightarrow & \langle p_2 - p_0, p_1 - p_2 \rangle \leq 0 \\
\Leftrightarrow & \underbrace{\langle p_2 - p_1, p_0 - p_2 \rangle}_{\geq 0 \text{ by Eq. (7)}} \leq 0.
\end{aligned}$$

$\square$

## B.2 Cubic Bézier Curves

**Lemma 3.** The two subcurves defined by their control points  $(p_0^L, p_1^L, p_2^L, p_3^L)$  and  $(p_0^R, p_1^R, p_2^R, p_3^R)$  resulting from de Cateljau subdivision [dC59] in the domain center of a cubic Bézier curve defined

by the control points  $(p_0, p_1, p_2, p_3)$  can be enclosed in disjoint bounding volumes partitioned by a plane located in the split point  $s := \frac{1}{8}(p_0 + 3p_1 + 3p_2 + p_3)$  and orthogonal to the tangent in the split point  $t := \frac{3}{4}(-p_0 - p_1 + p_2 + p_3)$  if

$$\langle p_2 - p_0, p_1 - p_0 \rangle \geq 0 \quad \text{and} \quad (10)$$

$$\langle p_3 - p_1, p_1 - p_0 \rangle \geq 0 \quad \text{and} \quad (11)$$

$$\langle p_3 - p_1, p_3 - p_2 \rangle \geq 0 \quad \text{and} \quad (12)$$

$$\langle p_2 - p_0, p_3 - p_2 \rangle \geq 0 \quad \text{and} \quad (13)$$

$$\langle p_2 - p_0, p_3 - p_1 \rangle \geq 0. \quad (14)$$

**Proof.** As a Bézier curve results from a convex combination of its control points, the bounding volumes of the two sub curves can disjointedly be split by the plane located in  $s$  and orthogonal to  $t$  if

$$\langle p_i^L - s, t \rangle \leq 0 \quad \text{and}$$

$$\langle p_i^R - s, t \rangle \geq 0 \quad \forall i \in \{0, 1, 2, 3\}.$$

De Casteljaou subdivision in the domain center creates the control points

$$(p_0^L, p_1^L, p_2^L, p_3^L) := \left( p_0, \frac{p_0 + p_1}{2}, \frac{p_0 + 2p_1 + p_2}{4}, \frac{p_0 + 3p_1 + 3p_2 + p_3}{8} \right) \quad \text{and}$$

$$(p_0^R, p_1^R, p_2^R, p_3^R) := \left( \frac{p_0 + 3p_1 + 3p_2 + p_3}{8}, \frac{p_1 + 2p_2 + p_3}{4}, \frac{p_2 + p_3}{2}, p_3 \right)$$

of the two subcurves.

Obviously  $p_3^L = p_0^R = s$  meet the conditions by construction with the given constraints<sup>1</sup>.

For  $p_2^L = \frac{p_0 + 2p_1 + p_2}{4}$

$$\begin{aligned} & \langle p_2^L - s, t \rangle \leq 0 \\ \Leftrightarrow & \left\langle \frac{p_0 + 2p_1 + p_2}{4} - \frac{p_0 + 3p_1 + 3p_2 + p_3}{8}, \frac{3(-p_0 - p_1 + p_2 + p_3)}{4} \right\rangle \leq 0 \\ \Leftrightarrow & \langle 2p_0 + 4p_1 + 2p_2 - (p_0 + 3p_1 + 3p_2 + p_3), -p_0 - p_1 + p_2 + p_3 \rangle \leq 0 \\ \Leftrightarrow & \underbrace{\langle p_0 + p_1 - p_2 - p_3, -p_0 - p_1 + p_2 + p_3 \rangle}_{\leq 0} \leq 0. \end{aligned}$$

For  $p_1^L = \frac{p_0 + p_1}{2}$

$$\begin{aligned} & \langle p_1^L - s, t \rangle \leq 0 \\ \Leftrightarrow & \left\langle \frac{p_0 + p_1}{2} - \frac{p_0 + 3p_1 + 3p_2 + p_3}{8}, \frac{3(-p_0 - p_1 + p_2 + p_3)}{4} \right\rangle \leq 0 \\ \Leftrightarrow & \langle 4p_0 + 4p_1 - (p_0 + 3p_1 + 3p_2 + p_3), -p_0 - p_1 + p_2 + p_3 \rangle \leq 0 \\ \Leftrightarrow & \langle 3p_0 + p_1 - 3p_2 - p_3, -p_0 - p_1 + p_2 + p_3 \rangle \leq 0 \\ \Leftrightarrow & \langle 3(p_2 - p_0) + (p_3 - p_1), (p_2 - p_0) + (p_3 - p_1) \rangle \geq 0 \\ \Leftrightarrow & 3 \underbrace{\langle p_2 - p_0, p_2 - p_0 \rangle}_{\geq 0} + 4 \underbrace{\langle p_2 - p_0, p_3 - p_1 \rangle}_{\geq 0 \text{ by Eq. (14)}} + \underbrace{\langle p_3 - p_1, p_3 - p_1 \rangle}_{\geq 0} \geq 0. \end{aligned}$$

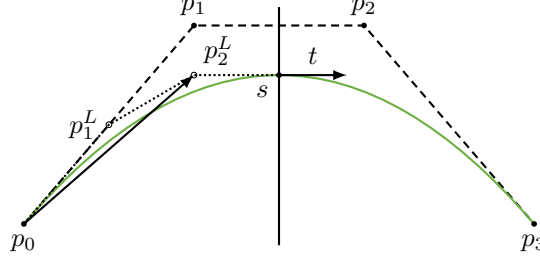


**Figure 10:**  $p_0$  must be located on the left side of the separation plane together with  $p_2^L$  if  $\langle p_2^L - p_0, t \rangle \geq 0$ .

Finally, knowing that  $p_2^L$  is already on the correct side of the splitting plane (see also Figure 10),  $p_0^L$  is on the same side of the plane if

$$\begin{aligned}
& \langle p_2^L - p_0^L, t \rangle \geq 0 \\
\Leftrightarrow & \left\langle \frac{p_0 + 2p_1 + p_2}{4} - p_0, \frac{3(-p_0 - p_1 + p_2 + p_3)}{4} \right\rangle \geq 0 \\
\Leftrightarrow & \langle -3p_0 + 2p_1 + p_2, -p_0 - p_1 + p_2 + p_3 \rangle \geq 0 \\
\Leftrightarrow & \langle 2(p_1 - p_0) + (p_2 - p_0), (p_2 - p_0) + (p_3 - p_1) \rangle \geq 0 \\
\Leftrightarrow & \underbrace{2 \langle p_1 - p_0, p_2 - p_0 \rangle}_{\geq 0 \text{ by Eq. (10)}} + \underbrace{2 \langle p_1 - p_0, p_3 - p_1 \rangle}_{\geq 0 \text{ by Eq. (11)}} \\
& \quad + \underbrace{\langle p_2 - p_0, p_2 - p_0 \rangle}_{\geq 0} + \underbrace{\langle p_2 - p_0, p_3 - p_1 \rangle}_{\geq 0 \text{ by Eq. (14)}} \geq 0.
\end{aligned}$$

For the right subcurve

$$\begin{aligned}
& \langle p_1^R - s, t \rangle \geq 0 \\
\Leftrightarrow & \left\langle \frac{p_1 + 2p_2 + p_3}{4} - \frac{p_0 + 3p_1 + 3p_2 + p_3}{8}, \frac{3(-p_0 - p_1 + p_2 + p_3)}{4} \right\rangle \geq 0 \\
\Leftrightarrow & \langle 2p_1 + 4p_2 + 2p_3 - p_0 - 3p_1 - 3p_2 - p_3, -p_0 - p_1 + p_2 + p_3 \rangle \geq 0 \\
\Leftrightarrow & \underbrace{\langle -p_0 - p_1 + p_2 + p_3, -p_0 - p_1 + p_2 + p_3 \rangle}_{\geq 0} \geq 0,
\end{aligned}$$

$$\begin{aligned}
& \langle p_2^R - s, t \rangle \geq 0 \\
\Leftrightarrow & \left\langle \frac{p_2 + p_3}{2} - \frac{p_0 + 3p_1 + 3p_2 + p_3}{8}, \frac{3(-p_0 - p_1 + p_2 + p_3)}{4} \right\rangle \geq 0 \\
\Leftrightarrow & \langle 4p_2 + 4p_3 - p_0 - 3p_1 - 3p_2 - p_3, -p_0 - p_1 + p_2 + p_3 \rangle \geq 0 \\
\Leftrightarrow & \langle -p_0 - 3p_1 + p_2 + 3p_3, -p_0 - p_1 + p_2 + p_3 \rangle \geq 0 \\
\Leftrightarrow & \langle (p_2 - p_0) + 3(p_3 - p_1), (p_2 - p_0) + (p_3 - p_1) \rangle \geq 0 \\
\Leftrightarrow & \underbrace{\langle p_2 - p_0, p_2 - p_0 \rangle}_{\geq 0} + \underbrace{4 \langle p_2 - p_0, p_3 - p_1 \rangle}_{\geq 0 \text{ by Eq. (14)}} + \underbrace{3 \langle p_3 - p_1, p_3 - p_1 \rangle}_{\geq 0} \geq 0,
\end{aligned}$$

<sup>1</sup>Note that the curves do touch in  $s$  and hence their bounding volumes would have a shared plane. In practice, we still work with disjoint bounding volumes by assigning everything on the partitioning plane explicitly to the subcurve tested first; the result obviously remains the same.

and again knowing that  $p_1^R$  is already on the correct side of the splitting plane,  $p_3^R$  is on the same side of the plane if

$$\begin{aligned}
& \langle p_3^R - p_1^R, t \rangle \geq 0 \\
\Leftrightarrow & \left\langle p_3 - \frac{p_1 + 2p_2 + p_3}{4}, \frac{3(-p_0 - p_1 + p_2 + p_3)}{4} \right\rangle \geq 0 \\
\Leftrightarrow & \langle -p_1 - 2p_2 + 3p_3, -p_0 - p_1 + p_2 + p_3 \rangle \geq 0 \\
\Leftrightarrow & \langle (p_3 - p_1) + 2(p_3 - p_2), (p_2 - p_0) + (p_3 - p_1) \rangle \geq 0 \\
\Leftrightarrow & \underbrace{\langle p_3 - p_1, p_2 - p_0 \rangle}_{\geq 0 \text{ by Eq. (14)}} + \underbrace{\langle p_3 - p_1, p_3 - p_1 \rangle}_{\geq 0} \\
& + 2 \underbrace{\langle p_3 - p_2, p_2 - p_0 \rangle}_{\geq 0 \text{ by Eq. (13)}} + 2 \underbrace{\langle p_3 - p_2, p_3 - p_1 \rangle}_{\geq 0 \text{ by Eq. (12)}} \geq 0.
\end{aligned} \tag{15}$$

Finally, as a Bézier curve is a convex combination of its control points, the curve is always enclosed in their convex hull, and therefore all subcurves in the two domains are completely on one side of the split plane each.  $\square$

**Lemma 4.** Splitting the cubic Bézier curve fulfilling the conditions (10), (11), (12), (13), (14) in the middle results in two subcurves that also satisfy them all. Hence, all nested subcurves from further bisection fulfill the conditions.

**Proof.** For the left subcurve

$$\begin{aligned}
& \langle p_2^L - p_0^L, p_1^L - p_0^L \rangle \geq 0 \\
\Leftrightarrow & \left\langle \frac{p_0 + 2p_1 + p_2}{4} - p_0, \frac{p_0 + p_1}{2} - p_0 \right\rangle \geq 0 \\
\Leftrightarrow & \left\langle \frac{-3p_0 + 2p_1 + p_2}{4}, \frac{p_1 - p_0}{2} \right\rangle \geq 0 \\
\Leftrightarrow & \langle -3p_0 + 2p_1 + p_2, p_1 - p_0 \rangle \geq 0 \\
\Leftrightarrow & \langle (p_2 - p_0) + 2(p_1 - p_0), p_1 - p_0 \rangle \geq 0 \\
\Leftrightarrow & \underbrace{\langle p_2 - p_0, p_1 - p_0 \rangle}_{\geq 0 \text{ by Eq. (10)}} + 2 \underbrace{\langle p_1 - p_0, p_1 - p_0 \rangle}_{\geq 0} \geq 0,
\end{aligned}$$
  

$$\begin{aligned}
& \langle p_3^L - p_1^L, p_1^L - p_0^L \rangle \geq 0 \\
\Leftrightarrow & \left\langle \frac{p_0 + 3p_1 + 3p_2 + p_3}{8} - \frac{p_0 + p_1}{2}, \frac{p_0 + p_1}{2} - p_0 \right\rangle \geq 0 \\
\Leftrightarrow & \left\langle \frac{-3p_0 - p_1 + 3p_2 + p_3}{8}, \frac{p_1 - p_0}{2} \right\rangle \geq 0 \\
\Leftrightarrow & \langle -3(p_2 - p_0) + (p_3 - p_1), p_1 - p_0 \rangle \geq 0 \\
\Leftrightarrow & -3 \underbrace{\langle p_2 - p_0, p_1 - p_0 \rangle}_{\geq 0 \text{ by Eq. (10)}} + \underbrace{\langle p_3 - p_1, p_1 - p_0 \rangle}_{\geq 0 \text{ by Eq. (11)}} \geq 0,
\end{aligned}$$

$$\begin{aligned}
& \langle p_3^L - p_1^L, p_3^L - p_2^L \rangle \geq 0 \\
\Leftrightarrow & \left\langle \frac{p_0 + 3p_1 + 3p_2 + p_3}{8} - \frac{p_0 + p_1}{2}, \frac{p_0 + 3p_1 + 3p_2 + p_3}{8} - \frac{p_0 + 2p_1 + p_2}{4} \right\rangle \geq 0 \\
\Leftrightarrow & \langle -3p_0 - p_1 + 3p_2 + p_3, -p_0 - p_1 + p_2 + p_3 \rangle \geq 0 \\
\Leftrightarrow & \langle 3(p_2 - p_0) + (p_3 - p_1), (p_2 - p_0) + (p_3 - p_1) \rangle \geq 0 \\
\Leftrightarrow & 3 \underbrace{\langle p_2 - p_0, p_2 - p_0 \rangle}_{\geq 0} + 4 \underbrace{\langle p_2 - p_0, p_3 - p_1 \rangle}_{\geq 0 \text{ by Eq. (14)}} + \underbrace{\langle p_3 - p_1, p_3 - p_1 \rangle}_{\geq 0} \geq 0,
\end{aligned}$$

$$\begin{aligned}
& \langle p_2^L - p_0^L, p_3^L - p_2^L \rangle \geq 0 \\
\Leftrightarrow & \left\langle \frac{p_0 + 2p_1 + p_2}{4} - p_0, \frac{p_0 + 3p_1 + 3p_2 + p_3}{8} - \frac{p_0 + 2p_1 + p_2}{4} \right\rangle \geq 0 \\
\Leftrightarrow & \langle -3p_0 + 2p_1 + p_2, -p_0 - p_1 + p_2 + p_3 \rangle \geq 0 \\
\Leftrightarrow & \langle (p_2 - p_0) + 2(p_1 - p_0), (p_2 - p_0) + (p_3 - p_1) \rangle \geq 0 \\
\Leftrightarrow & \underbrace{\langle p_2 - p_0, p_2 - p_0 \rangle}_{\geq 0} + \underbrace{\langle p_2 - p_0, p_3 - p_1 \rangle}_{\geq 0 \text{ by Eq. (14)}} \\
& + 2 \underbrace{\langle p_1 - p_0, p_2 - p_0 \rangle}_{\geq 0 \text{ by Eq. (10)}} + 2 \underbrace{\langle p_1 - p_0, p_3 - p_1 \rangle}_{\geq 0 \text{ by Eq. (11)}} \geq 0,
\end{aligned}$$

$$\begin{aligned}
& \langle p_2^L - p_0^L, p_3^L - p_1^L \rangle \geq 0 \\
\Leftrightarrow & \left\langle \frac{p_0 + 2p_1 + p_2}{4} - p_0, \frac{p_0 + 3p_1 + 3p_2 + p_3}{8} - \frac{p_0 + p_1}{2} \right\rangle \geq 0 \\
\Leftrightarrow & \langle -3p_0 + 2p_1 + p_2, p_0 + 3p_1 + 3p_2 + p_3 - 4p_0 - 4p_1 \rangle \geq 0 \\
\Leftrightarrow & \langle -3p_0 + 2p_1 + p_2, -3p_0 - p_1 + 3p_2 + p_3 \rangle \geq 0 \\
\Leftrightarrow & \langle 2(p_1 - p_0) + (p_2 - p_0), 3(p_2 - p_0) + (p_3 - p_1) \rangle \geq 0 \\
\Leftrightarrow & 6 \underbrace{\langle (p_1 - p_0), (p_2 - p_0) \rangle}_{\geq 0 \text{ by Eq. (10)}} + 2 \underbrace{\langle (p_1 - p_0), (p_3 - p_1) \rangle}_{\geq 0 \text{ by Eq. (11)}} \\
& + 3 \underbrace{\langle (p_2 - p_0), (p_2 - p_0) \rangle}_{\geq 0} + \underbrace{\langle (p_2 - p_0), (p_3 - p_1) \rangle}_{\geq 0 \text{ by Eq. (14)}} \geq 0.
\end{aligned}$$

For the right subcurve

$$\begin{aligned}
& \langle p_2^R - p_0^R, p_1^R - p_0^R \rangle \geq 0 \\
\Leftrightarrow & \left\langle \frac{p_2 + p_3}{2} - \frac{p_0 + 3p_1 + 3p_2 + p_3}{8}, \frac{p_1 + 2p_2 + p_3}{4} - \frac{p_0 + 3p_1 + 3p_2 + p_3}{8} \right\rangle \geq 0 \\
\Leftrightarrow & \langle -p_0 - 3p_1 + p_2 + 3p_3, -p_0 - p_1 + p_2 + p_3 \rangle \geq 0 \\
\Leftrightarrow & \langle 3(p_3 - p_1) + (p_2 - p_0), (p_3 - p_1) + (p_2 - p_0) \rangle \geq 0 \\
\Leftrightarrow & 3 \underbrace{\langle p_3 - p_1, p_3 - p_1 \rangle}_{\geq 0} + 4 \underbrace{\langle p_3 - p_1, p_2 - p_0 \rangle}_{\geq 0 \text{ by Eq. (14)}} + \underbrace{\langle p_2 - p_0, p_2 - p_0 \rangle}_{\geq 0} \geq 0,
\end{aligned}$$

$$\begin{aligned}
& \langle p_3^R - p_1^R, p_1^R - p_0^R \rangle \geq 0 \\
\Leftrightarrow & \left\langle p_3 - \frac{p_1 + 2p_2 + p_3}{4}, \frac{p_1 + 2p_2 + p_3}{4} - \frac{p_0 + 3p_1 + 3p_2 + p_3}{8} \right\rangle \geq 0 \\
\Leftrightarrow & \langle -p_1 - 2p_2 + 3p_3, -p_0 - p_1 + p_2 + p_3 \rangle \geq 0 \\
\Leftrightarrow & \langle (p_3 - p_1) + 2(p_2 - p_0), (p_3 - p_1) + (p_2 - p_0) \rangle \geq 0 \\
\Leftrightarrow & \underbrace{\langle p_3 - p_1, p_3 - p_1 \rangle}_{\geq 0} + \underbrace{\langle p_3 - p_1, p_2 - p_0 \rangle}_{\geq 0 \text{ by Eq. (14)}} \\
& + 2 \underbrace{\langle p_3 - p_2, p_3 - p_1 \rangle}_{\geq 0 \text{ by Eq. (12)}} + 2 \underbrace{\langle p_3 - p_2, p_2 - p_0 \rangle}_{\geq 0 \text{ by Eq. (13)}} \geq 0,
\end{aligned}$$

$$\begin{aligned}
& \langle p_3^R - p_1^R, p_3^R - p_2^R \rangle \geq 0 \\
\Leftrightarrow & \left\langle p_3 - \frac{p_1 - 2p_2 + p_3}{4}, p_3 - \frac{p_2 + p_3}{2} \right\rangle \geq 0 \\
\Leftrightarrow & \langle -p_1 - 2p_2 + 3p_3, -p_2 + p_3 \rangle \geq 0 \\
\Leftrightarrow & \langle 2(p_3 - p_2) + (p_3 - p_1), p_3 - p_2 \rangle \geq 0 \\
\Leftrightarrow & 2 \underbrace{\langle p_3 - p_2, p_3 - p_2 \rangle}_{\geq 0} + \underbrace{\langle p_3 - p_1, p_3 - p_2 \rangle}_{\geq 0 \text{ by Eq. (12)}} \geq 0,
\end{aligned}$$

$$\begin{aligned}
& \langle p_2^R - p_0^R, p_3^R - p_2^R \rangle \geq 0 \\
\Leftrightarrow & \left\langle \frac{p_2 + p_3}{2} - \frac{p_0 + 3p_1 + 3p_2 + p_3}{8}, p_3 - \frac{p_2 + p_3}{2} \right\rangle \geq 0 \\
\Leftrightarrow & \langle -p_0 - 3p_1 + p_2 + 3p_3, p_3 - p_2 \rangle \geq 0 \\
\Leftrightarrow & \langle 3(p_3 - p_1) + (p_2 - p_0), p_3 - p_2 \rangle \geq 0 \\
\Leftrightarrow & 3 \underbrace{\langle p_3 - p_1, p_3 - p_2 \rangle}_{\geq 0 \text{ by Eq. (12)}} + \underbrace{\langle p_2 - p_0, p_3 - p_2 \rangle}_{\geq 0 \text{ by Eq. (13)}} \geq 0,
\end{aligned}$$

$$\begin{aligned}
& \langle p_2^R - p_0^R, p_3^R - p_1^R \rangle \geq 0 \\
\Leftrightarrow & \left\langle \frac{p_2 + p_3}{2} - \frac{p_0 + 3p_1 + 3p_2 + p_3}{8}, p_3 - \frac{p_1 + 2p_2 + p_3}{4} \right\rangle \geq 0 \\
\Leftrightarrow & \langle -p_0 - 3p_1 + p_2 + 3p_3, 3p_3 - p_1 - 2p_2 \rangle \geq 0 \\
\Leftrightarrow & \langle 3(p_3 - p_1) + (p_2 - p_0), 2(p_3 - p_2) + (p_3 - p_1) \rangle \geq 0 \\
\Leftrightarrow & 6 \underbrace{\langle p_3 - p_1, p_3 - p_2 \rangle}_{\geq 0 \text{ by Eq. (12)}} + 3 \underbrace{\langle p_3 - p_1, p_3 - p_1 \rangle}_{\geq 0} \\
& + 2 \underbrace{\langle p_2 - p_0, p_3 - p_2 \rangle}_{\geq 0 \text{ by Eq. (13)}} + \underbrace{\langle p_2 - p_0, p_3 - p_1 \rangle}_{\geq 0 \text{ by Eq. (14)}} \geq 0.
\end{aligned}$$

□

## Appendix C: Intersection code

```
float intersect_plane(const vec3f p, const vec3f n)
{
    return dot3(n, p) / n.z;
}
```

**Listing 1:** Intersection of a unit ray with a plane through  $p$  with normal  $n$ .

```
tuple<float, float> intersect_cylinder
(
    const vec3f o,
    const vec3f a,
    const float r
)
{
    const float d = a.x * o.y - a.y * o.x;
    const float g = a.x * a.x + a.y * a.y;
    if (g == 0 && o.x * o.x + o.y * o.y < r * r)
        return make_tuple(-FLT_MAX, FLT_MAX);

    const float h = 1.0f / g;
    const float e = r * r - d * d * h;

    if (e < 0)
        return make_tuple(FLT_MAX, FLT_MAX);

    const float t_cpa = o.z - a.z * (a.x*o.x + a.y*o.y)*h;
    const float s = sqrtf(e * (a.z * a.z + g) * h);

    return make_tuple(t_cpa - s, t_cpa + s);
}
```

**Listing 2:** Intersection of a unit ray with an infinite cylinder with radius  $r$  through  $o$  along  $a$ .

```

float dist_2points_line
(
    const vec3f& p,
    const vec3f& q,
    const vec3f& d
)
{
    const float c = dot3(d, d);

    const float bp = dot3(p, d) / c;
    const vec3f pPbp = p - bp * d;
    const float l2_pPbp = dot3(pPbp, pPbp);

    const float bq = dot3(q, d) / c;
    const vec3f qPbq = q - bq * d;
    const float l2_qPbq = dot3(qPbq, qPbq);

    return sqrtf(max(l2_pPbp, l2_qPbq));
}

```

**Listing 3:** Maximum distance of the two points  $p, q$  to the line starting in the origin and going along  $d$ .

```

tuple<float, float> get_interval
(
    const int32_t start,
    const int32_t size
)
{
    const int32_t ui0 = 0x3f800000 | start;
    const float u0 = int_as_float(ui0) - 1.0f;
    const int32_t ui1 = min(ui0 + size, 0x40000000);
    const float u1 = int_as_float(ui1) - 1.0f;
    return make_tuple(u0, u1);
}

```

**Listing 4:** Conversion of the integer representation of the interval (start, size) to the floating point interval  $[u_0, u_1]$ .

```

vec4f eval(const BezierCurve c, const float u)
{
    float v = 1.0f - u;
    return v * v * v * c.p0
        + 3.0f * u * v * v * c.p1
        + 3.0f * u * u * v * c.p2
        + u * u * u * c.p3;
}

vec4f eval_derivative(const BezierCurve c, const float u)
{
    float v = 1.0f - u;
    return v * v * (c.p1 - c.p0)
        + 2.0f * u * v * (c.p2 - c.p1)
        + u * u * (c.p3 - c.p2);
}

```

**Listing 5:** Evaluate cubic Bézier curve and its (scaled) derivative.

```

BezierCurveDelta calculate_control_points
(
    const BezierCurve& c,
    const uint32_t     cur_start,
    const uint32_t     cur_size
)
{
    float u0, u1;
    tie(u0, u1) = get_interval(cur_start, cur_size);
    const vec4f p = eval(c, u0);
    const vec4f d = eval(c, u1) - p;
    const vec4f t0 = (u1 - u0) * eval_derivative(c, u0);
    const vec4f t1 = (u1 - u0) * eval_derivative(c, u1);
    return BezierCurveDelta(p, d, t0, t1);
}

```

**Listing 6:** Re-calculation of the cubic Bézier curve represented by the tuple  $(p, d, t_0, t_1)$  for an interval  $[u_0, u_1]$  used after backtracking.

```

void subdivide_and_set
(
    const bool         go_right,
    const vec4f&       center,
    const vec4f&       t_center,
    BezierCurveDelta& c
)
{
    if (go_right)
    {
        c.p += center;
        c.d -= center;
        c.t0 = t_center;
        c.t1 *= 0.5f;
    }
    else
    {
        c.d = center;
        c.t0 *= 0.5f;
        c.t1 = t_center;
    }
}

```

**Listing 7:** Subdivide the curve

```

float calculate_conservative_radius
(
    const BezierCurveDelta& c
)
{
    const float dist = dist_2points_line(c.t0.xyz(), c.t1.xyz(), c.d.xyz());
    const float max_r = c.p.w + max(max(0.0f, c.t0.w), max(c.d.w, c.d.w - c.t1.w));
    return dist + max_r;
}

```

**Listing 8:** Calculate a conservative radius of a cylinder bounding a cubic Bézier curve.

```

tuple<bool, bool> subdivide_partition_and_update
(
    const BezierCurveDelta& c,
    const float t0,
    const float t1,
    float& t_min,
    float& t_max
)
{
    vec4f center;
    vec4f t_center;
    tie(center, t_center) = c.get_center_and_tangent();
    const float t_plane = intersect_plane(c.p.xyz() + center.xyz(), t_center.xyz());

    const bool go_right = t_plane > t0 ^ t_center.z > 0;
    const bool both_hit = t0 < t_plane && t1 > t_plane;

    // Update t interval
    if (t_plane > t0) t_max = min(t_max, t_plane);
    else t_min = max(t_min, t_plane);

    // Subdivide
    subdivide_and_set(go_right, center, t_center, c);

    return make_tuple(both_hit, go_right);
}

```

**Listing 9:** Partition space, subdivide curve, and update state

```

tuple<float, float> calculate_t_interval
(
    const BezierCurveDelta& cur_c,
    const float ray_t_max
)
{
    const float t0 = intersect_plane(cur_c.p, cur_c.t0);
    const float t1 = intersect_plane(cur_c.p + cur_c.d, cur_c.t1);
    float t_min = 0.0f;
    if (cur_c.t0.z > 0) t_min = max(t_min, t0);
    if (cur_c.t1.z < 0) t_min = max(t_min, t1);
    float t_max = ray_t_max;
    if (cur_c.t0.z < 0) t_max = min(t_max, t0);
    if (cur_c.t1.z > 0) t_max = min(t_max, t1);

    return make_tuple(t_min, t_max);
}

```

**Listing 10:** Calculate the valid  $t$  interval between the cropping planes.

```

vec3f transform
(
    const vec3f& p,
    const vec3f& origin,
    const vec3f& u,
    const vec3f& v,
    const vec3f& w
)
{
    vec3f q = p - origin;
    return vec3f(dot3(q, u), dot3(q, v), dot3(q, w));
}

BezierCurve transform_to_ray_frame
(
    const vec3f& origin,
    const vec3f& direction,
    const BezierCurve& c
)
{
    const vec3f w = direction;
    vec3f u, v;
    tie(u, v) = make_ONB(w);

    return BezierCurve(transform(c.p0, origin, u, v, w),
                        transform(c.p1, origin, u, v, w),
                        transform(c.p2, origin, u, v, w),
                        transform(c.p3, origin, u, v, w));
}

```

**Listing 11:** Transform a cubic Bézier curve to a ray frame.

```

void go_down
(
    const bool both_hit,
    const bool go_right,
    uint32_t& cur_size,
    uint32_t& bit_string,
    uint32_t& cur_start
)
{
    cur_size /= 2;
    if (both_hit) bit_string ^= cur_size;
    if (go_right) cur_start ^= cur_size;
}

void jump_up
(
    uint32_t& cur_size,
    uint32_t& cur_start,
    uint32_t& bit_string
)
{
    // ctz = count trailing zeros
    cur_size = 1 << ctz(bit_string);
    cur_start ^= cur_size;
    bit_string ^= cur_size;
    cur_start &= ~(cur_size - 1);
}

```

**Listing 12:** Bit string manipulation to advance ~~24~~ the next finer level (go\_down) and for backtracking (jump\_up).

```

Intersection calculate_intersection
(
    const uint32_t          cur_start ,
    const uint32_t          cur_size ,
    const float            t ,
    const BezierCurve&      c ,
    const BezierCurveDelta& cur_c
)
{
    // Project intersection - p_0 onto p_n - p_0
    vec3f hb = cur_c.p.xyz() - vec3f(0, 0, t);
    float u_local = dot3(hb, cur_c.d.xyz());
    u_local /= dot3(cur_c.d.xyz(), cur_c.d.xyz());
    u_local = max(0.0f, min(1.0f, -u_local));

    float u0, u1;
    tie(u0, u1) = get_interval(cur_start, cur_size);
    float u = u0 + u_local * (u1 - u0);

    // End caps?
    if (u == 0.0f || u == 1.0f)
    {
        vec3f n = (u == 0.0f ? c.p0.xyz() : c.p3.xyz()) -
                  (u == 0.0f ? c.p1.xyz() : c.p2.xyz());
        return Intersection(t, u, normalize3(n));
    }

    vec3f ap = cur_c.p.xyz() + u_local * cur_c.axis;

    // Recompute frame
    vec3f frame_u, frame_v;
    tie(frame_u, frame_v) = make_ONB(ray_direction);

    // Caclulate normal in global frame
    vec3f normal = normalize3(t * ray_direction - ap.x * frame_u - ap.y * frame_v -
ap.z * ray_direction);

    return Intersection(t, u, normal);
}

```

**Listing 13:** Calculate the normal and  $u$  parameter in the intersection.

```

Intersection intersect
(
    const Ray&          ray,
    const BezierCurve& c,
    const uint32_t      min_size,
)
{
    // State
    const BezierCurve c_local = transform_to_ray_frame(ray.origin, ray.direction, c);
    BezierCurveDelta cur_c     = c_local; // conversion {p0, p1, p2, p3} -> {p, d, t0,
    t1}
    float t                    = FLT_MAX;
    uint32_t bit_string        = 0;
    uint32_t cur_size          = 1 << 23;
    uint32_t cur_start         = 0;
    float t_min, t_max;

    // Set the initial t interval
    tie(t_min, t_max) = calculate_t_interval(cur_c, ray.t_max);

    while (true)
    {
        const float cur_r = calculate_conservative_radius(cur_c);

        float t0, t1;
        tie(t0, t1) = intersect_cylinder(cur_c.p, cur_c.d, cur_r);
        if (t1 >= t_min && t0 <= t_max)
        {
            if (cur_size <= min_size)
            {
                t = t0;
                break;
            }

            // Subdivide and go down in the hierarchy
            bool both_hit, go_right;
            tie(both_hit, go_right) = subdivide_partition_and_update(cur_c, t0, t1, t_min,
t_max);
            go_down(both_hit, go_right, cur_size, bit_string, cur_start);
        }
        else
        {
            // Done?
            if (!bit_string) break;

            // Backtracking
            jump_up(cur_size, cur_start, bit_string);
            cur_c = calculate_control_points(c_local, cur_start, cur_size);

            // Re-calculate the t interval
            tie(t_min, t_max) = calculate_t_interval(cur_c);
        }
    }

    // Calculate normal etc. if a closer intersection has been found
    if (t < ray.t_max)
        return calculate_intersection(cur_start, cur_size, t, c, cur_c);
    else
        return Intersection(); // no intersection
}

```

**Listing 14:** Iterative routine for ray/fiber intersection using recursive subdivision with disjoint bounding volumes.